# Coversheet for EarthArXiv

**Title:**

Worldwide consequences of a mid-Holocene cooling in the Nordic Seas

**Authors:**

*M M Telesiński* – Institute of Oceanology Polish Academy of Sciences, Powstańców Warszawy 55, Sopot 81-712, Poland

*W Liu* – Department of Earth and Planetary Sciences, University of California Riverside, Riverside, CA, USA

*X Ren* – Department of Earth and Planetary Sciences, University of California Riverside, Riverside, CA, USA

*M Zajączkowski* – Institute of Oceanology Polish Academy of Sciences, Powstańców Warszawy 55, Sopot 81-712, Poland

**Author Email Addresses:**

*M M Telesiński (mtelesinski@iopan.pl)*

*W Liu (wei.liu@ucr.edu)*

*X Ren (xianglin.ren@email.ucr.edu)*

*M Zajączkowski (trapper@iopan.pl)*

**Peer Review Statement:**

**Title: Worldwide consequences of a mid-Holocene cooling in the Nordic Seas**

**Author names and affiliations**

Maciej M. Telesiński[a], Wei Liu[b], Xianglin Ren[b], Marek Zajączkowski[a]

[a]Institute of Oceanology Polish Academy of Sciences, Powstańców Warszawy 55, Sopot 81-712, Poland

[b]Department of Earth and Planetary Sciences, University of California Riverside, Riverside, CA, USA

**Teaser:** The secrets of a 6.8 ka BP cooling event reshape our understanding of ancient climates and their impact on the future.

**The Earth's climate, marked by long-term shifts and punctuated events, shapes terrestrial and marine ecosystems. Despite the present interglacial period's warmth and stability compared to preceding glaciations, the Holocene has witnessed significant cooling events with worldwide consequences. Leveraging marine records from the Nordic Seas, we provide the first detailed account of a cooling event centered around 6.8 ka BP. Utilizing paleoceanographic proxies and advanced modelling, we unveil a distinct subsurface water cooling, associated with a stepwise increase in sea-ice cover in the eastern Fram Strait. Our findings emphasize the role of Greenland Sea deep convection onset and the subsequent westward shift in Atlantic Water flow, enabling sea-ice advection from the Barents Sea. The heightened sea-ice cover weakens Atlantic Water advection, perturbing overturning circulation in the eastern Nordic Seas. These perturbations propagate worldwide, affecting North Atlantic deep-water circulation, inducing widespread hemispheric cooling, shifting the Intertropical Convergence Zone southward, and weakening the East Asian monsoon. Incorporating rigorous modelling**

**supports and augments proxy-based paleoreconstructions, underscoring sea-ice dynamics and ocean circulation's critical influence. This study highlights the potential for localized cooling events within ostensibly stable climatic intervals, underscoring the need to comprehend their mechanisms for precise climate predictions and informed policymaking toward a sustainable future.**

## Introduction

The present interglacial (*1*) is a relatively warm and stable interval in terms of environmental conditions, especially when compared with the last glacial period (*2*) marked by Dansgaard-Oeschger events, or Greenland interstadials (*3*, *4*), and Greenland stadials recorded both in marine and terrestrial archives. However, several prominent cooling events have been identified within the Holocene (*5*, *6*). Some of them were proven to be of regional or overregional importance (*5*, *7*). Bond et al. (*8*) suggested a millennial-scale cyclicity of North Atlantic cooling episodes, expressed mainly as phases of increased ice rafting in the region. However, cyclicity has later been questioned (*9*) as different dynamical processes seem to have played a major role in the particular events (*5*).

Three climate oscillations were recorded in the early Holocene section of Greenland ice cores (*10*). These include the well-known 8.2 ka BP event (*11–13*), the 9.3 ka event of shorter duration but almost similar amplitude (*8*, *14*, *15*), and the Preboreal Oscillation during the Holocene's first centuries (*16*, *17*). The expression of these cold relapses can also be found in marine sediment records (*6*, *7*, *18–20*). Another worldwide climate deterioration occurred at 2.7 ka BP (*21*) and was most probably caused by a perturbation of the Atlantic Meridional Overturning Circulation (AMOC) (*22*, *23*), initiated by a solar irradiance anomaly (*24*) and a subsequent disruption of deep convection in the Nordic Seas (*25*).

Wanner et al. (*5*) identified six cold relapses that interrupted periods of more stable and warmer climate over the last 10,000 years. These events, recorded in time series of temperature and humidity/precipitation and identified at least in the extratropical area of the Northern Hemisphere, were centered around 8.2, 6.3, 4.7, 2.7, 1.55 and 0.55 ka BP, thus roughly correlating to Bond events 0-5.

In this paper, we focus on the interval between 7 and 6 ka BP, generally regarded as one of the warmest intervals of the Holocene in the Northern Hemisphere, during which substantial cooling of subsurface waters is observed in several marine sediment records along the North Atlantic Drift (NAD) in the Nordic Seas. This event, centered around 6.8 ka BP, correlates roughly with the onset of cooling trends observed in different parts of the world (*5*, *7*, *26*). We investigate whether the subsurface cooling in the Nordic Seas might have acted as a trigger for a worldwide cooling event using both proxy paleorecords and modelling results.

## Results

An increase in the relative abundance of *N. pachyderma* can be observed between ~8.5 and 8 ka BP in most of the records used in this study (Fig. 2). The increase in the abundance of this polar species indicates a widespread cooling of the subsurface water (Fig. 3) associated with the 8.2 ka BP event (*20*, *27*). The signal was particularly strong in the Norwegian Sea cores (MD95-2011, M17730 and M23258). In the Fram Strait, the 8.2 ka BP event had a lower amplitude, and already around 8 ka BP rapid warming occurred, peaking around 7.8-7.9 ka BP. This is in agreement with recent studies on the origin of the 8.2 ka BP event, indicating an increase in freshwater input into the Labrador Sea and a decrease in AW export from the subpolar gyre into the Nordic Seas (*28*, *29*). As the event originated southwest of the Nordic Seas, it seems obvious that the southern part of the region was more affected than its northern part.

Shortly after the warm rebound, the sSST in the Nordic Seas started to decrease again (Fig. 3). After ~7 ka BP, a further abrupt cooling occurred, culminating around 6.8 ka BP. Although the age uncertainty for individual records around that time ranges from 470 years (core MSM5/5-712) to 1460 years (core OCE2017-GR02), the mean ages of the peak cooling fall within an interval of fewer than 300 years (6.6-6.9 ka BP), giving us confidence that both the age models of individual cores and the overall chronological framework of the study are correct. Only ~6 ka BP the sSST increased to levels comparable to those before 7 ka BP. In almost all the records, the cooling had a similar amplitude of roughly 1.5°C. Only in the southernmost record, MD95-2011 can no cooling of such an amplitude be found. However, the transfer function used here reconstructs temperatures at a water depth of 10 m (*27*), compared to 100 m in most of the other records (Table 2). This, together with a prominent increase in the abundance of *N. pachyderma* between 7 and 6.5 ka BP (Fig. 2) might suggest that the cooling occurred deeper (100 m), while not affecting shallower waters (~10 m) in the central Norwegian Sea. In core MSM5/5-712 from the eastern Fram Strait, the cooling was twofold, with peaks centered around 6.8 and 6.1 ka BP. Originally, these were described as two separate events (*6*). However, the sSST remained lower between the two peaks than before and after them, implying that the two peaks are two phases of the same event. With the available data, it is difficult to determine why the event was twofold only at this specific location.

Despite a similar amplitude in all the records, the cold spell was the most pronounced in the Fram Strait records (Fig. 3), where it stands out as the most prominent cooling event over the Holocene. A cooling of comparable amplitude seems to be recorded also in core OCE2017-GR02 from the continental slope of NE Greenland. This record is of notably lower temporal resolution. As a result, the age of the peak cooling falls within the interval of 5.9-7.4 ka BP (95% confidence range), slightly broader than in other records (95% confidence range of 6.4-7.1 ka BP). However, a similar amplitude of the cooling and a fair age overlap with the other records strongly suggest that the 6.8 ka BP cooling reached the NE Greenland continental slope. In the southernmost records (MD95-2011 and M17730), the cooling seems to be less pronounced, especially when compared to other Holocene temperature variations, e.g., the 8.2 ka BP event (Figs. 2 and 3). The different size fractions and transfer functions used for temperature reconstructions might at least partly explain the difference in the amplitude of the faunal and sSST changes between the records. However, they did not influence the relative differences in the amplitudes of the 6.8 ka BP event compared to, e.g., the 8.2 ka BP event in individual records. Taking into account all these indications, we can conclude that the 6.8 ka BP cooling originated in the Fram Strait, as it was most prominently recorded there.

The sSST decrease between 7 and 6 ka BP was accompanied by changes in other proxies from the records used in this study. Most notably, a stepwise increase of the $P_BIP_{25}$ index in core MSM5/5-723 (*30*) around 7 ka BP (Fig. 4B) indicates an increase in sea-ice cover (*31*). The increase is one of the most prominent features of the $P_BIP_{25}$ index record and the largest rise of this proxy over the Holocene. Furthermore, it was preceded by a stable interval of ~1 kyr and followed by a gradual, roughly linear increase that lasted until the end of the record. This suggests that it was one of the major shifts in the sea-ice cover in the Fram Strait during the present interglacial. In the same record, the fragmentation of planktic foraminifera increased around 7 ka BP (Fig. 4C), indicating the increased impact of cold, corrosive Arctic surface waters on the study area (*30*). The enhanced dissolution of planktic foraminiferal tests in the Fram Strait might also partly explain the particularly high percentages of *N. pachyderma* in this area, as thin-walled tests of subpolar species (e.g., *T. quinqueloba*) can be dissolved more easily in a corrosive environment than the thick-walled specimens of *N. pachyderma* (*32*). Both in the Fram Strait (core JM10-330) and the Norwegian Sea (cores M17730 and MD95-2011), a distinct decrease in planktic foraminiferal abundance occurred between 7 and 6 ka BP (Fig. 4D), which might also be related to the increased dissolution of foraminiferal tests. Ice rafting in the Fram Strait (core MSM5/5-712) intensified between 7 and 6 ka BP (Fig. 4E) further suggesting an increasing influence of Arctic waters. Meanwhile, the alkenone-based reconstruction from the northern Norwegian Sea (*33*) shows that the interval during which the subsurface cooling occurred was one of the warmest within the Holocene in terms of sea-surface temperatures (Fig. 4F), in line with the September insolation at 78°N (Fig. 4A). Given the transfer function used in core M23258 reconstructs sSST at 10 m water depth (*34*), the data from this core suggest an increased temperature gradient of the uppermost water column, at least in the northern Norwegian Sea (Fig. 1).

The results of the TraCE-21ka simulation show an increase of sea-ice concentration in the eastern Fram Strait (where cores MSM5/5-723, JM10-330 and MSM5/5-712 are located) and southwestern Barents Sea in the interval 6.83-6.85 ka BP compared to 7.63-7.65 ka BP (Fig. 5A). In contrast, in the southeastern Nordic Seas and in the northern North Atlantic, the sea-ice concentration decreased over that period and in the central and northwestern Nordic Seas it remained largely unchanged. A resulting sSST (around 100 m water depth) decrease can be observed two decades later (6.81-6.83 ka BP) in almost entire Nordic Seas, though predominantly on their eastern margin and in the Barents Sea, while the sSST increased south of the Greenland-Scotland Ridge (Fig. 5B). These results are in good agreement with the proxy-based paleoreconstructions presented above, especially in terms of geographical distribution of the described changes. It should be noted, however, that the subsurface cooling seems to be weaker in model than in the proxy records (~0.6°C vs. ~1.5°C). This discrepancy can be explained by the fact that the model shows changes in annual temperatures (and sea-ice concentrations) (*35*), which could be smaller than changes in summer temperatures reconstructed by the transfer functions (*36*, *37*). Other model biases cannot be excluded.

## Discussion

The middle part of the Holocene is generally considered the warmest and most stable interval of the present interglacial. It was characterized by high summer temperatures in the mid- and high-latitude areas of the Northern Hemisphere (*5*, *38–42*). Although the June insolation, which is the strongest in the Northern Hemisphere, was already in decline (*43*), the July and August insolation was still quite high, while the September insolation reached its maximum only around 6 ka BP (Fig. 4A). Furthermore, large ice sheets delaying ocean warming through katabatic winds and meltwater discharge were mostly gone (*44–46*) or became mainly land-based (*47*, *48*) in the middle Holocene. This is well reflected in sea-surface temperature (*33*, *49*, *50*) (Fig. 4F) and terrestrial records (*51*) covering this interval. Depending on the region and paleoenvironmental proxies used, large discrepancies exist in the boundaries of the warmest phase of the Holocene (*52*, *53*). However, regardless of the exact timing of the middle Holocene (*5*, *39*, *40*, *54*), the interval between 7 and 6 ka BP falls within most of its definitions. Thus, this time interval can be regarded as the warmest part of the present interglacial, at least in the mid- and high latitudes of the Northern Hemisphere. Despite this, distinct subsurface water cooling of approximately 1.5°C is observed along the NAD, suggesting a decrease in AW advection into the Nordic Seas.

After the 8.2 ka event, the AW inflow into the eastern Nordic Seas resumed, as shown by the sSST increase in all the discussed records (Fig. 2). The Iceland-Scotland Overflow Water flow speed also shows a distinct increase around that time (*22*). This indicates an intensification of the overturning circulation in the Nordic Seas probably related to the end of the widespread meltwater discharge from the Greenland Ice Sheet (GIS) (*47*) and the subsequent onset of deep convection in the Greenland Sea (*55*, *56*). However, since the main AW flow has been shifted towards the Greenland Sea (*55*), cooling can be observed starting shortly thereafter, especially in cores located farther north (M23258-2 and in the Fram Strait). The initial subsurface water cooling might have enabled a stepwise sea-ice expansion in the eastern Fram Strait that occurred around 7 ka BP (Fig. 4B). Increased sea-ice cover, in turn, must have influenced surface waters. Distinct surface water cooling can be observed in core JM09-020 from Storfjordrenna, south of Svalbard (*50*) (Fig. 4F), suggesting that the sea ice was advected into the eastern Fram Strait from the western Barents Sea. Further south, however, no sign of cooling can be observed (*33*, *49*, *57*), indicating that the surface temperature decrease was limited roughly to the sea-ice-covered area.

In contrast, for subsurface waters, the expansion of sea-ice cover had much more far-reaching implications. Increased sea-ice cover enhanced further stepwise subsurface cooling of approximately 1.5°C (Fig. 3) by acting as a positive feedback mechanism (*58*), i.e., by strengthening the halocline and causing the AW to sink deeper below it. The subsurface water cooling culminated around 6.8 ka BP. Despite a similar amplitude in all the records, it was the most pronounced in the Fram Strait, where it appears to be the most prominent subsurface cooling event over the Holocene. However, it was clearly marked in all records along the NAD from the central Norwegian Sea to the NW Greenland Sea. The results of the TraCE-21ka simulation also seem to confirm that the subsurface water cooling was induced by sea ice as they show an increase in sea-ice concentration in the eastern Fram Strait prior to the sSST decrease in the Nordic Seas, mostly in their eastern part (Fig. 5).

Such a strong subsurface water cooling presumably associated with a disruption of AW advection in a region as important for ocean circulation as the Nordic Seas could have had far-reaching consequences. Indeed, several studies, which we discuss below, report environmental perturbations that occurred after ~6.5 ka BP and might have had a causal link with the described cooling event.

A trend of decreasing contribution of high-$\delta^{13}$C North Atlantic Deep Water (NADW) relative to low-$\delta^{13}$C Southern Ocean Water (SOW) that began at about 6.5 ka BP and culminated around 5 ka BP (Fig. 6C) was recorded in the subpolar NE North Atlantic (*26*). A decrease in NADW contribution in the NE North Atlantic suggests that, despite active deep convection in the Greenland Sea (*55*), the overturning circulation in the eastern Nordic Seas was weakened, most probably by the described decrease in AW advection into this area. Further consequences that are being linked with the decreasing contribution of NADW in the NE North Atlantic (*26*) include meteorological conditions at high latitudes which were especially winter-like (i.e., more similar to those during the YD and the glacial) from 6.1 to 5.0 ka BP. This is indicated by high sea-salt sodium flux in Greenland ice-core data (Fig. 6D), suggesting enhanced storminess (*59*, *60*). Finally, a large proportion of cold, relatively fresh, ice-bearing surface water entering the NE North Atlantic from north of Iceland is indicated by a high relative abundance of hematite-stained grains (indicating that they originated from sedimentary deposits in Svalbard and eastern Greenland containing red beds) and other drift ice petrologic tracers (Fig. 6E) in sedimentary records from this area (Bond event 4) (*7*). This is also in agreement with a decrease in AW advection from the North Atlantic into the Nordic Seas. All three indications (*7*, *26*, *59*) suggest that the interval between ~6.5 and 5 ka BP was one of the most severe climate events of the Holocene. This interval can be directly linked to the 6.8 ka BP event in the Nordic Seas not only because of the temporal convergence but also because the Nordic Seas are a key area for the AMOC, one of the most important mechanisms regulating both oceanic and climatic environmental changes in the North Atlantic region (*61*). Indeed, the results of the TraCE-21ka simulation show a slowdown of the AMOC (Fig. 7A) and a reduction of Atlantic cross-equatorial heat transport (Fig. 7B) directly after the 6.8 ka BP event (6.5-6.2 ka BP). As indicated by previous modelling studies (*62*, *63*), such a perturbation in overturning circulation might bring large-scale climate responses: prominent cooling over the northern North Atlantic and neighbouring areas, sea-ice increases over the Nordic Seas and to the south of Greenland, and a significant southward rain-belt migration over the tropical Atlantic. The latter is also confirmed by the TraCE-21ka simulation (Fig. 7C). The model shows that the slowdown of the AMOC and the reduction of Atlantic cross-equatorial heat transport between ~6.5 ka BP and ~6.2 ka BP lead to a southward shift of the Intertropical Convergence Zone (ITCZ). According to the zonal mean precipitation change, the southward shift is manifested by a general decrease in rainfall to the north of the equator and an increase in rainfall to the south of the equator. This dipole change in rainfall is especially pronounced over the Atlantic sector.

Based on the carefully selected Holocene time series of temperature and humidity/precipitation, as well as reconstructions of glacier advances, Wanner et al. (*5*) analysed the spatiotemporal pattern of six cold relapses of widespread reach during the last 10,000 years. One of the identified events occurred within the Holocene Thermal Maximum, between 6.5 and 5.9 ka BP. It was characterised by a predominance of negative temperature anomalies in the Southern Hemisphere (Fig. 6F). Similarly, the inner area of North America was cool (*64*) (Fig. 6G), in contrast to the area around Scandinavia where a majority of positive temperature anomalies occurred during this time. Especially the latter might seem surprising in the face of the cooling described here. However, first of all, the widespread event peaked at around 6.3 ka BP (*5*), i.e., ~400 years after the peak of cooling in the Nordic Seas. The cooling and its consequences propagated time-transgressively away from its source, and by the time the worldwide event reached its maximum, in the Nordic Seas the temperatures were already rising (Fig. 3). Second, cooling at 6.8 ka BP affected the subsurface water masses, while the surface waters were affected only locally, close to Svalbard (Fig. 4F). For this reason, the air temperatures around the Nordic Seas were not directly affected by the event.

Further indications suggest that a cold North Atlantic area and a southward shift of the ITCZ during the 6.5-5.9 ka BP cold relapse could have weakened the East Asian monsoon (*65*) (Fig. 6H). It is also suggested that reduced solar activity was at the origin of the 6.5-5.9 ka BP cold relapse (*5*). However, the solar irradiance minimum occurred at only ~6.3 ka BP (*66*). While we find it plausible that changes in solar activity could have amplified the cooling and enhanced its spreading across both hemispheres (*21*, *25*, *55*), it seems unrealistic to be a root cause as it occurred already within the cooling.

The described environmental changes that occurred during the 6.5-5 ka BP interval show how the consequences of a fairly local event such as the one at 6.8 ka BP in the Nordic Seas can potentially spread across both Hemispheres. Although a direct causal relationship between the 6.8 ka BP event and its worldwide implications might be difficult to prove and requires further studies, it certainly is possible, and the temporal convergence is very compelling. Furthermore, the results of the TraCE-21ka simulation seem to support such relationship. Therefore, we assume that the 6.8-ka BP event could have acted as a trigger for the worldwide cooling event.

The discussed sequence of events has important implications for the present-day environmental conditions and future predictions. It shows that even during a relatively warm and stable interval, a fairly local cold spell can occur, and its consequences can spread across both hemispheres. The ongoing warming of the Arctic (*67–70*) is a harbinger of changes that will affect the entire planet (*71*). However, these changes do not necessarily have to be straightforward or uniform (*72*). Based on the paleoenvironmental proxy records and model simulations presented here, we suggest that, for example, increased meltwater input from Svalbard glaciers and the GIS caused by increasing air temperatures (*73*, *74*) could lead to a similar cooling as the one that occurred 6.8 ka BP with consequences reaching beyond the Nordic Seas (*75*, *76*). For this reason, paleoreconstructions of such events should be used as analogues for potential future developments of environmental changes. Furthermore, it should be tested whether climate models that are used for future climate predictions can resolve such complex feedbacks within the ocean-atmosphere system.

## Methods

For the study, we have selected seven previously published marine sedimentary records from the eastern and northern Nordic Seas of at least multi-centennial resolution. These include (Fig. 1) cores MD95-2011 (*27*), M17730 (*25*), M23258 (*34*), MSM5/5-712 (*6*), JM10-330 (*77*), MSM5/5-723 (*78*) and OCE2017-GR02 (*55*). Details of the cores are given in Table 1.

All radiocarbon ages were recalibrated using the Marine20 calibration curve (*79*) to create a coherent chronological framework. The age-depth relationships were modelled using a Bayesian approach with the Bacon software ver. 3.1.0 (*80*). A regional correction of $\Delta R = -149 \pm 31$ $^{14}C$ years was applied for all cores except OCE2017-GR02. This value was calculated with the Marine Reservoir Correction database (*81*) and the Marine20 curve (*79*, *82*) using the same whale bones samples as those used by Mangerud et al. (*83*). For core OCE2017-GR02 no regional correction was used (*55*, *84*). Details on the age-depth relationships are given in Supplementary Fig. 1.

While the four planktic foraminiferal records from the Fram Strait (OCE2017-GR02, MSM5/5-723, JM10-330 and MSM5/5-712) are based on the >100 µm fraction, the records from further south (M23258, M17730 and MD95-2011) are based on the >150 µm fraction, which may bias the comparison of planktic foraminiferal assemblages. Subpolar species, e.g., *Turborotalita quinqueloba*, typically reach smaller test sizes in the polar North Atlantic, so the records based on smaller fractions are more sensitive to changes in Atlantic Water (AW) inflow (e.g., *85*). To mitigate this discrepancy, we have used transfer functions adequate to the size fraction used in each record to obtain absolute subsurface water temperatures (sSST). In most cases, we used previously published sSST reconstructions (*25*, *27*, *30*, *34*). In cores OCE2017-GR02 and JM10-330, we have calculated the sSST using the transfer function of Husum and Hald (*36*) and the C2 software, version 1.8.0 (*86*). Details on the sSST reconstructions are given in Table 2. To facilitate the comparison of the records, they were smoothed using LOESS regression with a span depending on their average Holocene temporal resolution (i.e., higher resolution records were averaged over a larger number of data points than the lower resolution records), to obtain an average resolution of approximately 500 years. Both raw and smoothed data are presented.

The Transient simulation of Climate Evolution of the last 21,000 years (TraCE-21ka) is carried out using a fully coupled climate model, the Community Climate System Model Version 3 (CCSM3), with a dynamic global vegetation module (*35*). The CCSM3 ocean component has a nominal horizontal resolution of 3° and 25 vertical levels, while the atmosphere component has a horizontal resolution of about 3.75° and 26 vertical hybrid coordinate levels. TraCE-21ka is driven by changes in meltwater fluxes, ice sheet extents, greenhouse gas concentrations, and orbital parameters. It is capable of well simulating the climate changes that occurred during the last deglaciation (*87–90*). The TraCE-21ka decadal annual mean output is available. In this study, we compare sea-ice concentrations and subsurface water temperatures (at 92 m water depth) between the peak cooling in the Nordic Seas (6.83-6.85 ka BP and 6.81-6.83 ka BP, respectively) and an interval before the cooling (7.63-7.65 ka BP). We also analyse the time series of AMOC strength and Atlantic cross-equatorial ocean heat transport over the Holocene as well as the worldwide precipitation difference between 6.18-6.27 ka BP and 6.50-6.59 ka BP in the TraCE-21ka simulation.

## References

1. M. J. C. Walker, S. J. Johnsen, S. O. Rasmussen, T. Popp, J. P. Steffensen, P. L. Gibbard, W. Hoek, J. Lowe, J. T. Andrews, S. Björck, L. C. Cwynar, K. A. Hughen, P. Kershaw, B. Kromer, T. Litt, D. J. Lowe, T. Nakagawa, R. Newnham, J. Schwander, Formal definition and dating of the GSSP (Global Stratotype Section and Point) for the base of

the Holocene using the Greenland NGRIP ice core, and selected auxiliary records. *J. Quat. Sci.* **24**, 3–17 (2009).

2. K. K. Andersen, N. Azuma, J.-M. Barnola, M. Bigler, P. Biscaye, N. Caillon, J. Chappellaz, H. B. Clausen, D. Dahl-Jensen, H. Fischer, J. Flückiger, D. Fritzsche, Y. Fujii, K. Goto-Azuma, K. Grønvold, N. S. Gundestrup, M. E. Hansson, C. Huber, C. S. Hvidberg, S. J. Johnsen, U. Jonsell, J. Jouzel, S. Kipfstuhl, A. Landais, M. Leuenberger, R. Lorrain, V. Masson-Delmotte, H. Miller, H. Motoyama, H. Narita, T. Popp, S. O. Rasmussen, D. Raynaud, R. Rothlisberger, U. Ruth, D. Samyn, J. Schwander, H. Shoji, M.-L. Siggard-Andersen, J. P. Steffensen, T. F. Stocker, A. E. Sveinbjörnsdottir, A. M. Svensson, M. Takata, J.-L. Tison, T. Thorsteinsson, O. Watanabe, F. Wilhelms, J. W. C. White, High-resolution record of Northern Hemisphere climate extending into the last interglacial period. *Nature*. **431**, 147–151 (2004).

3. S. J. Johnsen, H. B. Clausen, W. Dansgaard, K. Fuhrer, N. S. Gundestrup, C. U. Hammer, P. Iversen, J. Jouzel, B. Stauffer, J. P. Steffensen, Irregular glacial interstadials recorded in a new Greenland ice core. *Nature*. **359**, 311–313 (1992).

4. W. Dansgaard, S. J. Johnsen, H. B. Clausen, D. Dahl-Jensen, N. S. Gundestrup, C. U. Hammer, C. S. Hvidberg, J. P. Steffensen, A. E. Sveinbjörnsdottir, J. Jouzel, G. C. Bond, Evidence for general instability of past climate from a 250-kyr ice-core record. *Nature*. **364**, 218–220 (1993).

5. H. Wanner, O. Solomina, M. Grosjean, S. P. Ritz, M. Jetel, Structure and origin of Holocene cold events. *Quat. Sci. Rev.* **30**, 3109–3123 (2011).

6. K. Werner, R. F. Spielhagen, D. Bauch, H. C. Hass, E. S. Kandiano, Atlantic Water advection versus sea-ice advances in the eastern Fram Strait during the last 9 ka: Multiproxy evidence for a two-phase Holocene. *Paleoceanography*. **28**, 283–295 (2013).

7. G. C. Bond, B. Kromer, J. Beer, R. Muscheler, M. N. Evans, W. Showers, S. Hoffmann, R. Lotti-Bond, I. Hajdas, G. Bonani, Persistent solar influence on North Atlantic climate during the Holocene. *Science (80-. ).* **294**, 2130–2136 (2001).

8. G. C. Bond, W. Showers, M. Cheseby, R. Lotti, P. Almasi, P. DeMenocal, P. Priore, H. Cullen, I. Hajdas, G. Bonani, A Pervasive Millennial-Scale Cycle in North Atlantic Holocene and Glacial Climates. *Science (80-. ).* **278**, 1257–1266 (1997).

9. S. P. Obrochta, H. Miyahara, Y. Yokoyama, T. J. Crowley, A re-examination of evidence for the North Atlantic " 1500-year cycle" at Site 609. *Quat. Sci. Rev.* **55**, 23–33 (2012).

10. S. O. Rasmussen, B. M. Vinther, H. B. Clausen, K. K. Andersen, Early Holocene climate oscillations recorded in three Greenland ice cores. *Quat. Sci. Rev.* **26**, 1907–1914 (2007).

11. R. B. Alley, A. M. Ágústsdóttir, The 8k event: Cause and consequences of a major Holocene abrupt climate change. *Quat. Sci. Rev.* **24**, 1123–1149 (2005).

12. E. J. Rohling, H. Pälike, Centennial-scale climate cooling with a sudden cold event around 8,200 years ago. *Nature*. **434**, 975–979 (2005).

13. A. P. Wiersma, H. Renssen, Model-data comparison for the 8.2 ka BP event: Confirmation of a forcing mechanism by catastrophic drainage of Laurentide Lakes. *Quat. Sci. Rev.* **25**, 63–88 (2006).

14. U. Von Grafenstein, H. Erlenkeuser, A. Brauer, J. Jouzel, S. J. Johnsen, A mid-European decadal isotope-climate record from 15,500 to 5000 years B.P. *Science (80-. ).* **284**, 1654–1657 (1999).

15. F. McDermott, D. P. Mattey, C. Hawkesworth, Centennial-scale Holocene climate variability revealed by a high-resolution speleothem δ18O record from SW Ireland. *Science (80-. ).* **294** (2001), doi:10.1126/science.1063678.

16. S. Björck, M. Rundgren, Ó. Ingólfsson, S. Funder, The Preboreal oscillation around the Nordic Seas : terrestrial and lacustrine responses. *J. Quat. Sci.* **12**, 455–465 (1997).

17. J. van der Plicht, B. van Geel, S. J. P. Bohncke, M. Blaauw, A. O. M. Speranza, R. Muscheler, S. Björck, The Preboreal climate reversal and a subsequent solar-forced climate shift. *J. Quat. Sci.* **19**, 263–269 (2004).

18. M. M. Telesiński, J. E. Przytarska, B. Sternal, M. Forwick, W. Szczuciński, M. Łącka, M. Zajączkowski, Palaeoceanographic evolution of the SW Svalbard shelf over the last 14 000 years. *Boreas*. **47**, 410–422 (2018).

19. B. Sternal, W. Szczuciński, M. Forwick, M. Zajączkowski, S. Lorenc, J. E. Przytarska, Postglacial variability in near-bottom current speed on the continental shelf off south-west Spitsbergen. *J. Quat. Sci.* **29**, 767–777 (2014).

20. M. Hald, C. Andersson, H. Ebbesen, E. Jansen, D. Klitgaard-Kristensen, B. Risebrobakken, G. R. Salomonsen, M. Sarnthein, H. Petter, R. J. Telford, Variations in temperature and extent of Atlantic Water in the northern North Atlantic during the Holocene. *Quat. Sci. Rev.* **26**, 3423–3440 (2007).

21. B. van Geel, C. J. Heusser, H. Renssen, C. J. E. Schuurmans, Climatic change in Chile at around 2700 BP and global evidence for solar forcing: A hypothesis. *The Holocene*. **10**, 659–664 (2000).

22. I. R. Hall, G. G. Bianchi, J. R. Evans, Centennial to millennial scale Holocene climate-deep water linkage in the North Atlantic. *Quat. Sci. Rev.* **23**, 1529–1536 (2004).

23. D. J. R. Thornalley, H. Elderfield, I. N. McCave, Holocene oscillations in temperature and salinity of the surface subpolar North Atlantic. *Nature*. **457**, 711–4 (2009).

24. H. Renssen, H. Goosse, R. Muscheler, Coupled climate model simulation of Holocene

cooling events: oceanic feedback amplifies solar forcing. *Clim. Past*. **2**, 79–90 (2006).

25. M. M. Telesiński, H. A. Bauch, R. F. Spielhagen, E. S. Kandiano, Evolution of the central Nordic Seas over the last 20 thousand years. *Quat. Sci. Rev.* **121**, 98–109 (2015).

26. D. W. Oppo, J. F. McManus, J. L. Cullen, Deepwater variability in the Holocene epoch. *Nature*. **422**, 277–277 (2003).

27. B. Risebrobakken, E. Jansen, C. Andersson, E. Mjelde, K. Hevrøy, A high-resolution study of Holocene paleoclimatic and paleoceanographic changes in the Nordic Seas. *Paleoceanography*. **18**, 1017 (2003).

28. I. S. O. Matero, L. J. Gregoire, R. F. Ivanovic, J. C. Tindall, A. M. Haywood, The 8.2 ka cooling event caused by Laurentide ice saddle collapse. *Earth Planet. Sci. Lett.* **473**, 205–214 (2017).

29. A. Born, A. Levermann, The 8.2 ka event: Abrupt transition of the subpolar gyre toward a modern North Atlantic circulation. *Geochemistry, Geophys. Geosystems*. **11**, Q06011 (2010).

30. K. Werner, J. Müller, K. Husum, R. F. Spielhagen, E. S. Kandiano, L. Polyak, Holocene sea subsurface and surface water masses in the Fram Strait - Comparisons of temperature and sea-ice reconstructions. *Quat. Sci. Rev.* (2015), doi:10.1016/j.quascirev.2015.09.007.

31. J. Müller, A. Wagner, K. Fahl, R. Stein, M. Prange, G. Lohmann, Towards quantitative sea ice reconstructions in the northern North Atlantic: A combined biomarker and numerical modelling approach. *Earth Planet. Sci. Lett.* **306**, 137–148 (2011).

32. S. Ofstad, K. Zamelczyk, K. Kimoto, M. Chierici, A. Fransson, T. L. Rasmussen, Shell density of planktonic foraminifera and pteropod species Limacina helicina in the Barents

Sea: Relation to ontogeny and water chemistry. *PLoS One*. **16**, e0249178 (2021).

33. B. Martrat, J. O. Grimalt, J. Villanueva, S. Van Kreveld, M. Sarnthein, Climatic dependence of the organic matter contributions in the north eastern Norwegian Sea over the last 15,000 years. *Org. Geochem.* **34**, 1057–1070 (2003).

34. M. Sarnthein, S. van Kreveld, H. Erlenkeuser, P. M. Grootes, M. Kucera, U. Pflaumann, M. Schulz, Centennial-to-millennial-scale periodicities of Holocene climate and sediment injections off the western Barents shelf, 75°N. *Boreas*. **32**, 447–461 (2003).

35. F. He, thesis, University of Wisconsin-Madison (2011).

36. K. Husum, M. Hald, Arctic planktic foraminiferal assemblages: Implications for subsurface temperature reconstructions. *Mar. Micropaleontol.* **96**–**97**, 38–47 (2012).

37. U. Pflaumann, M. Sarnthein, M. R. Chapman, L. D’Abreu, B. Funnel, M. Huels, T. Kiefer, M. A. Maslin, H. Schulz, J. Swallow, S. van Kreveld, M. Vautravers, E. Vogelsang, M. S. Weinelt, Glacial North Atlantic: Sea-surface conditions reconstructed by GLAMAP 2000. *Paleoceanography*. **18**, 1065 (2003).

38. K. D. Alverson, T. F. Pedersen, R. S. Bradley, *Paleoclimate, Global Change and the Future* (Springer Berlin Heidelberg New York, Berlin Heidelberg New York, Global Cha., 2003; https://link.springer.com/book/10.1007/978-3-642-55828-3).

39. H. Renssen, H. Seppä, O. Heiri, D. M. Roche, H. Goosse, T. Fichefet, The spatial and temporal complexity of the Holocene thermal maximum. *Nat. Geosci.* **2**, 411–414 (2009).

40. H. Wanner, J. Beer, J. Bütikofer, T. J. Crowley, U. Cubasch, J. Flückiger, H. Goosse, M. Grosjean, F. Joos, J. O. Kaplan, M. Küttel, S. A. Müller, I. C. Prentice, O. Solomina, T. F. Stocker, P. Tarasov, M. Wagner, M. Widmann, Mid- to Late Holocene climate

change: an overview. *Quat. Sci. Rev.* **27**, 1791–1828 (2008).

41. E. S. Deevey, R. F. Flint, Postglacial Hypsithermal Interval. *Science (80-. ).* **125**, 182–184 (1957).

42. A. Nesje, M. Kvamme, Holocene glacier and climate variations in western Norway: Evidence for early Holocene glacier demise and multiple Neoglacial events. *Geology*. **19**, 610–612 (1991).

43. J. Laskar, P. Robutel, F. Joutel, M. Gastineau, a. C. M. Correia, B. Levrard, A long-term numerical solution for the insolation quantities of the Earth. *Astron. Astrophys.* **428**, 261–285 (2004).

44. A. Hormes, E. F. Gjermundsen, T. L. Rasmussen, From mountain top to the deep sea - Deglaciation in 4D of the northwestern Barents Sea ice sheet. *Quat. Sci. Rev.* **75**, 78–99 (2013).

45. S. P. Jessen, T. L. Rasmussen, T. Nielsen, A. Solheim, A new Late Weichselian and Holocene marine chronology for the western Svalbard slope 30,000-0 cal years BP. *Quat. Sci. Rev.* **29**, 1301–1312 (2010).

46. J. I. Svendsen, J. Mangerud, Holocene glacial and climatic variations on Spitsbergen, Svalbard. *The Holocene*. **7**, 45–57 (1997).

47. M.-S. Seidenkrantz, H. Ebbesen, S. Aagaard-Sørensen, M. Moros, J. M. Lloyd, J. Olsen, M. F. Knudsen, A. Kuijpers, Early Holocene large-scale meltwater discharge from Greenland documented by foraminifera and sediment parameters. *Palaeogeogr. Palaeoclimatol. Palaeoecol.* **391**, 71–81 (2012).

48. B. M. Vinther, S. L. Buchardt, H. B. Clausen, D. Dahl-Jensen, S. J. Johnsen, D. A. Fisher, R. M. Koerner, D. Raynaud, V. Lipenkov, K. K. Andersen, T. Blunier, S. O. Rasmussen,

J. P. Steffensen, A. M. Svensson, Holocene thinning of the Greenland ice sheet. *Nature*. **461**, 385–388 (2009).

49. E. Calvo, J. O. Grimalt, E. Jansen, High resolution U37K sea surface temperature reconstruction in the Norwegian Sea during the Holocene. *Quat. Sci. Rev.* **21**, 1385–1394 (2002).

50. M. Łącka, M. Cao, A. Rosell-Melé, J. Pawłowska, M. Kucharska, M. Forwick, M. Zajączkowski, Postglacial paleoceanography of the western Barents Sea: Implications for alkenone-based sea surface temperatures and primary productivity. *Quat. Sci. Rev.* **224** (2019), doi:10.1016/j.quascirev.2019.105973.

51. A. J. Thompson, J. Zhu, C. J. Poulsen, J. E. Tierney, C. B. Skinner, Northern Hemisphere vegetation change drives a Holocene thermal maximum. *Sci. Adv.* **8**, 1–11 (2022).

52. D. S. Kaufman, T. A. Ager, N. J. Anderson, P. M. Anderson, J. T. Andrews, P. J. Bartlein, L. B. Brubaker, L. L. Coats, L. C. Cwynar, M. L. Duvall, A. S. Dyke, M. E. Edwards, W. R. Eisner, K. Gajewski, A. Geirsdóttir, F. S. Hu, A. E. Jennings, M. R. Kaplan, M. W. Kerwin, A. V. Lozhkin, G. M. MacDonald, G. H. Miller, C. J. Mock, W. W. Oswald, B. L. Otto-Bliesner, D. F. Porinchu, K. Rühland, J. P. Smol, E. J. Steig, B. B. Wolfe, Holocene thermal maximum in the western Arctic (0-180°W). *Quat. Sci. Rev.* **23**, 529–560 (2004).

53. J. P. Briner, N. P. McKay, Y. Axford, O. Bennike, R. S. Bradley, A. de Vernal, D. Fisher, P. Francus, B. Fréchette, K. Gajewski, A. Jennings, D. S. Kaufman, G. Miller, C. Rouston, B. Wagner, Holocene climate change in Arctic Canada and Greenland. *Quat. Sci. Rev.* **147**, 340–364 (2016).

54. M. J. C. Walker, M. J. Head, J. Lowe, M. Berkelhammer, S. BjÖrck, H. Cheng, L. C. Cwynar, D. Fisher, V. Gkinis, A. Long, R. Newnham, S. O. Rasmussen, H. Weiss,

Subdividing the Holocene Series/Epoch: formalization of stages/ages and subseries/subepochs, and designation of GSSPs and auxiliary stratotypes. *J. Quat. Sci.* **34**, 173–186 (2019).

55. M. M. Telesiński, M. Łącka, A. Kujawa, M. Zajączkowski, The significance of Atlantic Water routing in the Nordic Seas: The Holocene perspective. *The Holocene*. **32**, 1104–1116 (2022).

56. D. J. R. Thornalley, M. Blaschek, F. J. Davies, S. Praetorius, D. W. Oppo, J. F. McManus, I. R. Hall, H. Kleiven, H. Renssen, I. N. McCave, Long-term variations in Iceland–Scotland overflow strength during the Holocene. *Clim. Past*. **9**, 2073–2084 (2013).

57. B. Risebrobakken, M. Moros, E. V. Ivanova, N. Chistyakova, R. Rosenberg, Climate and oceanographic variability in the SW Barents Sea during the Holocene. *The Holocene*. **20**, 609–621 (2010).

58. H. Gildor, E. Tziperman, P. W. Nienow, J. G. Shepherd, R. B. Alley, J. H. Lawton, A. Mahadevan, T. M. Lenton, Sea-ice switches and abrupt climate change. *Philos. Trans. R. Soc. A Math. Phys. Eng. Sci.* **361**, 1935–1944 (2003).

59. S. R. O'Brien, P. A. Mayewski, L. D. Meeker, D. A. Meese, M. S. Twickler, S. I. Whitlow, Complexity of Holocene Climate as Reconstructed from a Greenland Ice Core. *Science (80-. ).* **270**, 1962–1964 (1995).

60. R. H. Rhodes, X. Yang, E. W. Wolff, Sea Ice Versus Storms: What Controls Sea Salt in Arctic Ice Cores? *Geophys. Res. Lett.* **45**, 5572–5580 (2018).

61. W. E. Johns, M. O. Baringer, L. M. Beal, S. A. Cunningham, T. Kanzow, H. L. Bryden, J. J. M. Hirschi, J. Marotzke, C. S. Meinen, B. Shaw, R. Curry, Continuous, Array-Based

Estimates of Atlantic Ocean Heat Transport at 26.5°N. *J. Clim.* **24**, 2429–2449 (2011).

62. W. Liu, S. P. Xie, Z. Liu, J. Zhu, Overlooked possibility of a collapsed Atlantic Meridional Overturning Circulation in warming climate. *Sci. Adv.* **3**, 1–8 (2017).

63. W. Liu, A. V. Fedorov, S. P. Xie, S. Hu, Climate impacts of a weakened Atlantic Meridional Overturning Circulation in a warming climate. *Sci. Adv.* **6**, 1–9 (2020).

64. A. E. Viau, K. Gajewski, M. C. Sawada, P. Fines, Millennial-scale temperature variations in North America during the Holocene. *J. Geophys. Res. Atmos.* **111**, 1–12 (2006).

65. J. Xiao, Z. Chang, R. Wen, D. Zhai, S. Itoh, Z. Lomtatidze, Holocene weak monsoon intervals indicated by low lake levels at Hulun Lake in the monsoonal margin region of northeastern Inner Mongolia, China. *Holocene*. **19**, 899–908 (2009).

66. M. Vonmoos, J. Beer, R. Muscheler, Large variations in Holocene solar activity: Constraints from 10Be in the Greenland Ice Core Project ice core. *J. Geophys. Res.* **111**, A10105 (2006).

67. N. P. McKay, D. S. Kaufman, An extended Arctic proxy temperature database for the past 2,000 years. *Sci. Data*. **1**, 1–10 (2014).

68. R. F. Spielhagen, K. Werner, S. Aagaard-Sørensen, K. Zamelczyk, E. S. Kandiano, G. Budéus, K. Husum, T. M. Marchitto, M. Hald, Enhanced Modern Heat Transfer to the Arctic by Warm Atlantic Water. *Science (80-. ).* **331**, 450–453 (2011).

69. W. Walczowski, J. Piechura, Pathways of the Greenland Sea warming. *Geophys. Res. Lett.* **34**, 5 (2007).

70. Q. Schiermeier, Polar research: The new face of the Arctic. *Nature*. **446**, 133–135 (2007).

71. C. A. Boulton, L. C. Allison, T. M. Lenton, Early warning signals of Atlantic Meridional

Overturning Circulation collapse in a fully coupled climate model. *Nat. Commun.* **5**, 5752 (2014).

72. J. Cohen, X. Zhang, J. Francis, T. Jung, R. Kwok, J. E. Overland, T. J. Ballinger, U. S. Bhatt, H. W. Chen, D. Coumou, S. Feldstein, H. Gu, D. Handorf, G. Henderson, M. Ionita, M. Kretschmer, F. Laliberte, S. Lee, H. W. Linderholm, W. Maslowski, Y. Peings, K. Pfeiffer, I. Rigor, T. Semmler, J. Stroeve, P. C. Taylor, S. Vavrus, T. Vihma, S. Wang, M. Wendisch, Y. Wu, J. Yoon, Divergent consensuses on Arctic amplification influence on midlatitude severe winter weather. *Nat. Clim. Chang.* **10**, 20–29 (2020).

73. M. R. van den Broeke, E. M. Enderlin, I. M. Howat, P. Kuipers Munneke, B. P. Y. Noël, W. Jan Van De Berg, E. Van Meijgaard, B. Wouters, On the recent contribution of the Greenland ice sheet to sea level change. *Cryosphere*. **10**, 1933–1946 (2016).

74. S. Hetzinger, J. Halfar, Z. Zajacz, M. Möller, M. Wisshak, Late twentieth century increase in northern Spitsbergen (Svalbard) glacier-derived runoff tracked by coralline algal Ba/Ca ratios. *Clim. Dyn.* **56**, 3295–3303 (2021).

75. S. Rahmstorf, J. E. Box, G. Feulner, M. E. Mann, A. Robinson, S. Rutherford, E. J. Schaffernicht, Exceptional twentieth-century slowdown in Atlantic Ocean overturning circulation. *Nat. Clim. Chang.* **5** (2015), doi:10.1038/nclimate2554.

76. Q. Yang, T. H. Dixon, P. G. Myers, J. Bonin, D. Chambers, M. R. van den Broeke, M. H. Ribergaard, J. Mortensen, Recent increases in Arctic freshwater flux affects Labrador Sea convection and Atlantic overturning circulation. *Nat. Commun.* **7**, 10525 (2016).

77. C. Consolaro, T. L. Rasmussen, G. Panieri, J. Mienert, S. Bünz, K. Sztybor, Carbon isotope (d13C) excursions suggest times of major methane release during the last 14 kyr in Fram Strait, the deep-water gateway to the Arctic. *Clim. Past*. **11**, 669–685 (2015).

78. J. Müller, K. Werner, R. Stein, K. Fahl, M. Moros, E. Jansen, Holocene cooling culminates in sea ice oscillations in Fram Strait. *Quat. Sci. Rev.* **47**, 1–14 (2012).

79. T. J. Heaton, P. Köhler, M. Butzin, E. Bard, R. W. Reimer, W. E. N. Austin, C. B. Ramsey, P. M. Grootes, K. A. Hughen, B. Kromer, P. J. Reimer, J. F. Adkins, A. Burke, M. S. Cook, J. Olsen, L. C. Skinner, Marine20 — the Marine Radiocarbon Age Calibration Curve (0 – 55,000 Cal Bp). *Radiocarbon*. **00**, 1–42 (2020).

80. M. Blaauw, J. A. Christen, Flexible paleoclimate age-depth models using an autoregressive gamma process. *Bayesian Anal.* **6**, 457–474 (2011).

81. P. J. Reimer, R. W. Reimer, A marine reservoir correction database and on-line interface. *Radiocarbon*. **43**, 461–463 (2001).

82. T. J. Heaton, E. Bard, C. Bronk Ramsey, M. Butzin, C. Hatté, K. A. Hughen, P. Köhler, P. J. Reimer, A RESPONSE TO COMMUNITY QUESTIONS ON THE MARINE20 RADIOCARBON AGE CALIBRATION CURVE: MARINE RESERVOIR AGES AND THE CALIBRATION OF 14 C SAMPLES FROM THE OCEANS. *Radiocarbon*. **00**, 1–27 (2022).

83. J. Mangerud, S. Bondevik, S. Gulliksen, A. Karin Hufthammer, T. Høisæter, Marine 14C reservoir ages for 19th century whales and molluscs from the North Atlantic. *Quat. Sci. Rev.* **25**, 3228–3245 (2006).

84. D. Devendra, M. Łącka, M. M. Telesiński, T. L. Rasmussen, K. Sztybor, M. Zajączkowski, Paleoceanography of the Northwestern Greenland Sea and Return Atlantic Current evolution, 35–4 kyr BP. *Glob. Planet. Change*, 103947 (2022).

85. E. S. Kandiano, H. A. Bauch, Implications of planktic foraminiferal size fractions for the glacial-interglacial paleoceanography of the polar North Atlantic. *J. Foraminifer. Res.*

**32**, 245–251 (2002).

86. S. Juggins, C2, Software for Ecological and Palaeoecological Data Analysis and Visualization (2011).

87. W. Liu, Z. Liu, J. Cheng, H. Hu, On the stability of the Atlantic meridional overturning circulation during the last deglaciation. *Clim. Dyn.* **44**, 1257–1275 (2015).

88. W. Liu, A. Hu, The role of the PMOC in modulating the deglacial shift of the ITCZ. *Clim. Dyn.* **45**, 3019–3034 (2015).

89. W. Liu, Z. Liu, S. Li, The Driving Mechanisms on Southern Ocean Upwelling Change during the Last Deglaciation. *Geosciences*. **11**, 266 (2021).

90. S. Li, W. Liu, Deciphering the Migration of the Intertropical Convergence Zone During the Last Deglaciation. *Geophys. Res. Lett.* **49** (2022), doi:10.1029/2022GL098806.

91. C. Consolaro, T. L. Rasmussen, G. Panieri, Palaeoceanographic and environmental changes in the eastern Fram Strait during the last 14,000 years based on benthic and planktonic foraminifera. *Mar. Micropaleontol.* **139**, 84–101 (2018).

92. E. J. Steig, D. L. Morse, E. D. Waddington, M. Stuiver, P. M. Grootes, P. A. Mayewski, M. S. Twickler, S. I. Whitlow, Wisconsinan and holocene climate history from an ice core at taylor dome, western ross embayment, antarctica. *Geogr. Ann. Ser. A, Phys. Geogr.* **82**, 213–235 (2000).

93. P. J. Reimer, W. E. N. Austin, E. Bard, A. Bayliss, P. G. Blackwell, C. Bronk Ramsey, M. Butzin, H. Cheng, R. L. Edwards, M. Friedrich, P. M. Grootes, T. P. Guilderson, I. Hajdas, T. J. Heaton, A. G. Hogg, K. A. Hughen, B. Kromer, S. W. Manning, R. Muscheler, J. G. Palmer, C. Pearson, J. van der Plicht, R. W. Reimer, D. A. Richards, E. M. Scott, J. R. Southon, C. S. M. Turney, L. Wacker, F. Adolphi, U. Büntgen, M.

Capano, S. M. Fahrni, A. Fogtmann-Schulz, R. Friedrich, P. Köhler, S. Kudsk, F. Miyake, J. Olsen, F. Reinig, M. Sakamoto, A. Sookdeo, S. Talamo, The IntCal20 Northern Hemisphere Radiocarbon Age Calibration Curve (0-55 cal kBP). *Radiocarbon*. **62**, 725–757 (2020).

94. U. Pflaumann, J. Duprat, C. Pujol, L. D. Labeyrie, SIMMAX: A modern analog technique to deduce Atlantic sea surface temperatures from planktonic foraminifera in deep-sea sediments. *Paleoceanography*. **11**, 15–35 (1996).

## Figure captions

**Fig. 1.** Location of cores used in the study (dots) as well as present-day surface (red and blue arrows) and deep water circulation are shown. AF – Arctic Front, EGC – East Greenland Current, JMC – Jan Mayen Current, NAC – North Atlantic Current, PF – Polar Front, RAC – Return Atlantic Current, WSC – West Spitsbergen Current.

**Fig. 2.** Relative abundance of polar planktic foraminiferal species *N. pachyderma* in records from the eastern and northern Nordic Seas. Increases in the abundance of *N. pachyderma* associated with the 6.8 ka BP event is marked with the blue shading.

**Fig. 3.** Absolute subsurface water temperatures (sSST) reconstructed using transfer functions in records from the eastern and northern Nordic Seas. Cooling associated with the 6.8 ka BP event is marked with the blue shading.

**Fig. 4.** Paleoenvironmental proxies indicating changes associated with the 6.8 ka BP event. A) Insolation at 78°N for June, July, August, and September (*43*). B) $P_BIP_{25}$ index derived from biomarker data from core MSM5/5-723 (*30*). C) Fragmentation of planktic foraminifera tests in core MSM5/5-723 (*30*). D) Planktic foraminiferal abundance in cores JM10-330 (*91*),

M17730 (*25*) and MD95-2011 (*27*). E) Ice-rafted debris flux in core MSM5/5-712 (*6*), F) Alkenone-based sea-surface temperature reconstructions from cores JM09-020 (*50*) and M23258 (*33*). The 6.8 ka BP event is marked with blue shading.

**Fig. 5.** (A) Sea-ice concentration difference between 6.83-6.85 ka BP and 7.63-7.65 ka BP (6.83-6.85 ka BP minus 7.63-7.65 ka BP) in the TraCE-21ka. (B) Subsurface (92 m) temperature difference between 6.81-6.83 ka BP and 7.63-7.65 ka BP (6.81-6.83 ka BP and 7.63-7.65 ka BP) in the TraCE-21ka.

**Fig. 6.** Paleoceanographic and paleoclimatic records depicting the 6.8 ka BP event and its potential consequences. A) $P_BIP_{25}$ index proxy for sea-ice cover in the eastern Fram Strait core MSM5/5-723 (*30*). B) Absolute summer subsurface water temperatures (sSST, 100 m water depth) in the eastern Fram Strait (core JM10-330) reconstructed using the transfer function (this study). C) Benthic $\delta^{13}C$ proxy record for the contribution of NADW in the NE Atlantic ODP site 980 (*26*). D) Sea salt sodium (ssNa) flux proxy record for storminess/winter-like conditions in central Greenland GISP2 core (*59*). E) North Atlantic stack of drift ice petrologic tracers (*7*). F) Oxygen isotope record from an ice core at Tylor Dome, Antarctica, as air temperature proxy (*92*). G) North American pollen-based July temperature anomaly record (*64*). H) Sand-fraction content proxy record for low lake levels linked with weak monsoon events in core HL06 from Hulun Lake, East Asia (*65*). Records C-H are plotted vs. their original age models. However, a recalibration of the HL06 record using Bayesian approach and the IntCal20 calibration curve (*93*) has not shown remarkable differences from the original age model. In records D and F kiloyears before AD 2000 (ka b2k) were transformed into kiloyears before AD 1950 (ka BP). The 6.8 ka BP event is marked with blue shading.

**Fig. 7.** Time series of (A) AMOC strength and (B) Atlantic cross-equatorial ocean heat transport in the TraCE-21ka. (C) Precipitation difference between 6.18-6.27 ka BP and 6.50-6.59 ka BP (6.18-6.27 ka BP minus 6.50-6.59 ka BP) in the TraCE-21ka. 1 PW = 1 Petawatt = $10^{15}$ Watt

## Tables

**Table 1.** Details on cores used in the study. KAL – Kastenlot core, PC – piston core, GC – gravity core.

| Core ID | Latitude | Longitude | Water depth [m] | Core type | Location | References |
|---|---|---|---|---|---|---|
| **OCE2017-GR02** | 77°05' N | 5°20' W | 1200 | GC | NW Greenland Sea | Telesiński et al. 2022, Devendra et al. 2022 |
| **MSM5/5-723** | 79°09' N | 5°20' E | 1350 | KAL | E Fram Strait | Müller et al. 2012, Werner et al. 2015 |
| **JM10-330** | 79°08' N | 5°36' E | 1297 | GC | E Fram Strait | Consolaro et al. 2015, 2018 |
| **MSM5/5-712** | 78°55′ N | 6°46′ E | 1491 | KAL | E Fram Strait | Müller et al. 2012, Werner et al. 2013 |
| **M23258** | 75°00' N | 13°58' E | 1768 | KAL | N Norwegian Sea | Sarnthein et al. 2003, Martrat et al. 2003 |
| **M17730** | 72°07' N | 07°23' E | 2749 | KAL | N Norwegian Sea | Telesiński et al. 2015 |
| **MD95-2011** | 66°58' N | 07°38' E | 1048 | PC | central Norwegian Sea | Risebrobakken et al. 2003 |

**Table 2.** Details on the absolute temperature reconstructions used in the study. Uncertainties of the reconstructions are given as in the original references. RMSEP – root mean-squared error of prediction, SD – standard deviation.

| Core ID | Transfer function | Water depth [m] | Season | Uncertainty | Reference |
|---|---|---|---|---|---|
| **OCE2017-GR02** | (*36*) | 100 | summer | RMSEP = 0.52°C | this study |
| **MSM5/5-723-2** | (*36*) | 100 | summer | RMSEP = 0.47°C | Werner et al. 2015 |
| **JM10-330GC** | (*36*) | 100 | summer | RMSEP = 0.52°C | this study |
| **MSM5/5-712-2** | (*36*) | 100 | summer | RMSEP = 0.52°C | Werner et al. 2015 |
| **M23258** | (*37*, *94*) | 10 | summer | ±0.9°C | Sarnthein et al. 2003 |
| **M17730-4** | (*37*) | 100 | summer | SD = 0.3-2.2°C | Telesiński et al. 2015 |
| **MD95-2011** | (*37*) | 10 | August | unknown | Risobrobakken et al. 2003 |

Fig. 1

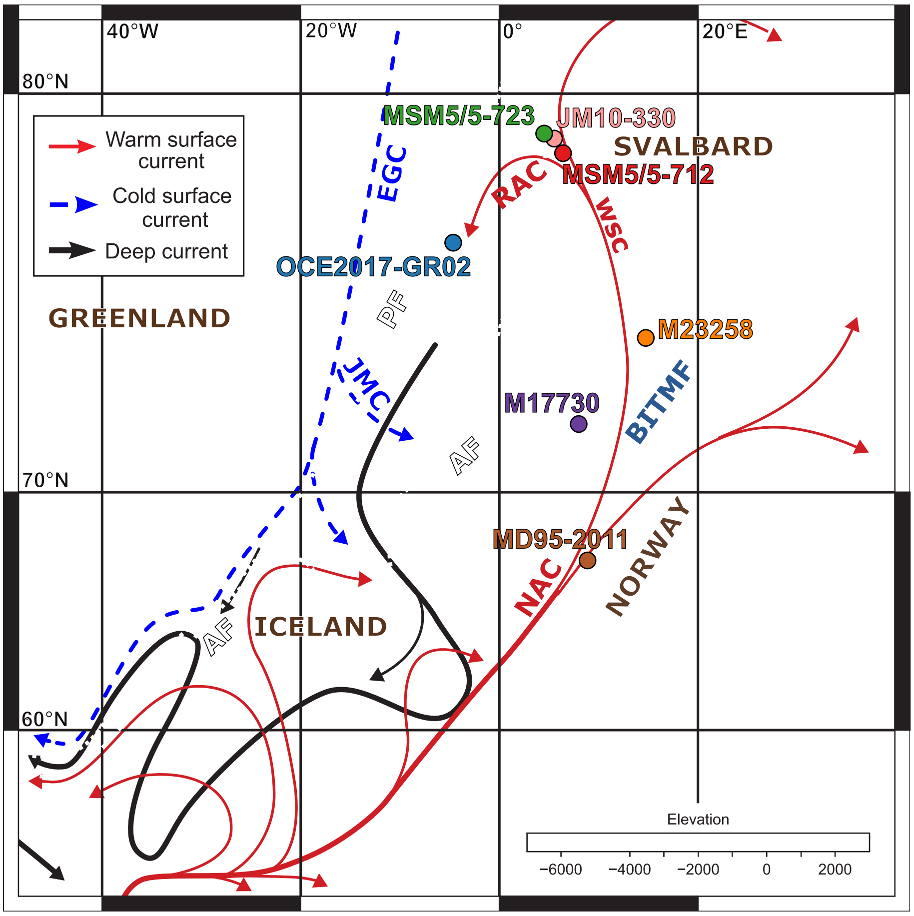

40°W
20°W
0°
20°E
80°N
70°N
60°N
Warm surface current
Cold surface current
Deep current
MSM5/5-723
JM10-330
SVALBARD
MSM5/5-712
RAC
WSC
EGC
OCE2017-GR02
GREENLAND
PF
M23258
JMC
M17730
BITMF
AF
MD95-2011
NAC
NORWAY
ICELAND
AF
Elevation
−6000
−4000
−2000
0
2000

Fig. 2

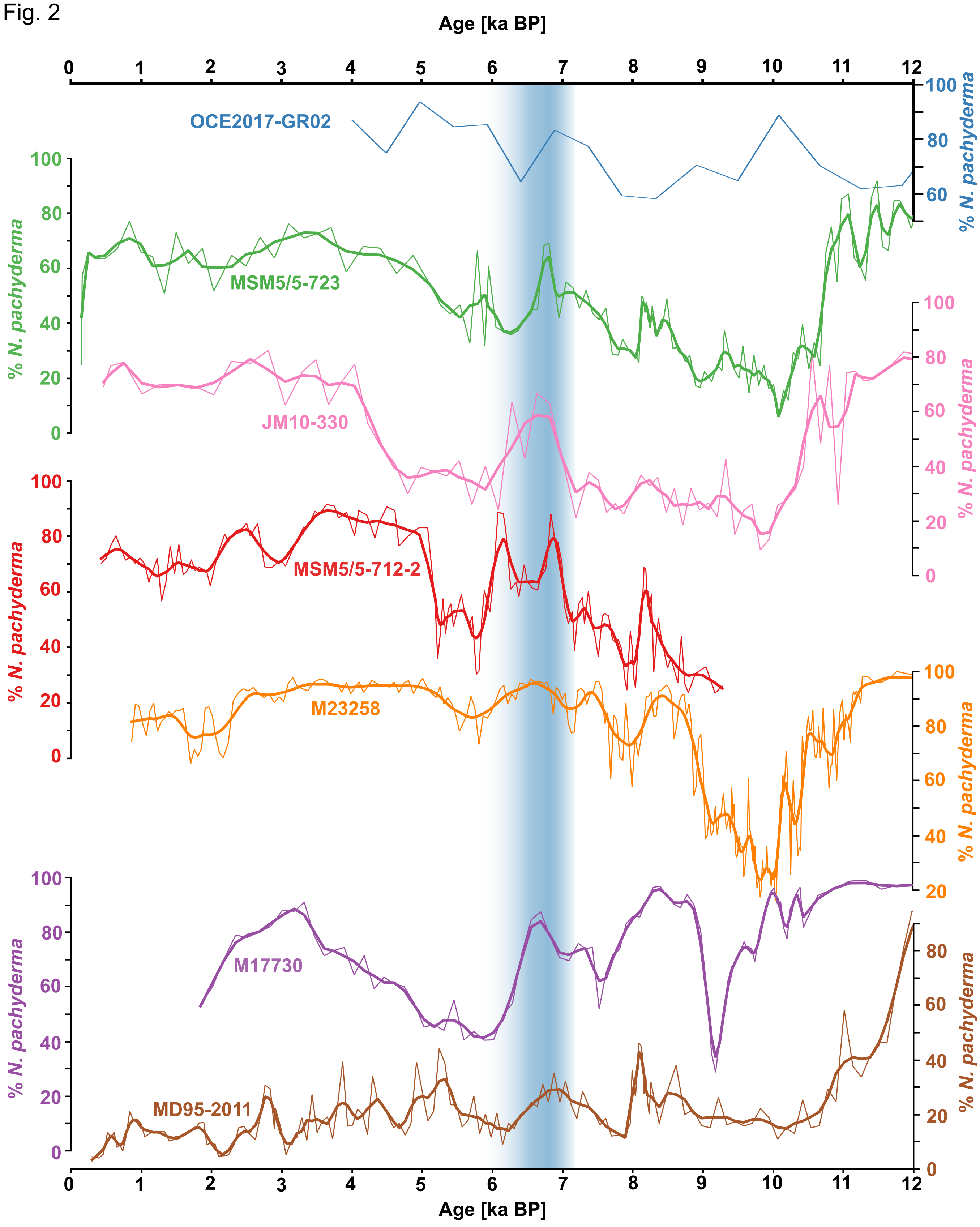

Age [ka BP]
0 1 2 3 4 5 6 7 8 9 10 11 12
OCE2017-GR02
% N. pachyderma
100 80 60
MSM5/5-723
% N. pachyderma
100 80 60 40 20 0
JM10-330
% N. pachyderma
100 80 60 40 20 0
MSM5/5-712-2
% N. pachyderma
100 80 60 40 20 0
M23258
% N. pachyderma
100 80 60 40 20
M17730
% N. pachyderma
100 80 60 40 20 0
MD95-2011
% N. pachyderma
80 60 40 20 0
0 1 2 3 4 5 6 7 8 9 10 11 12
Age [ka BP]

Fig. 3

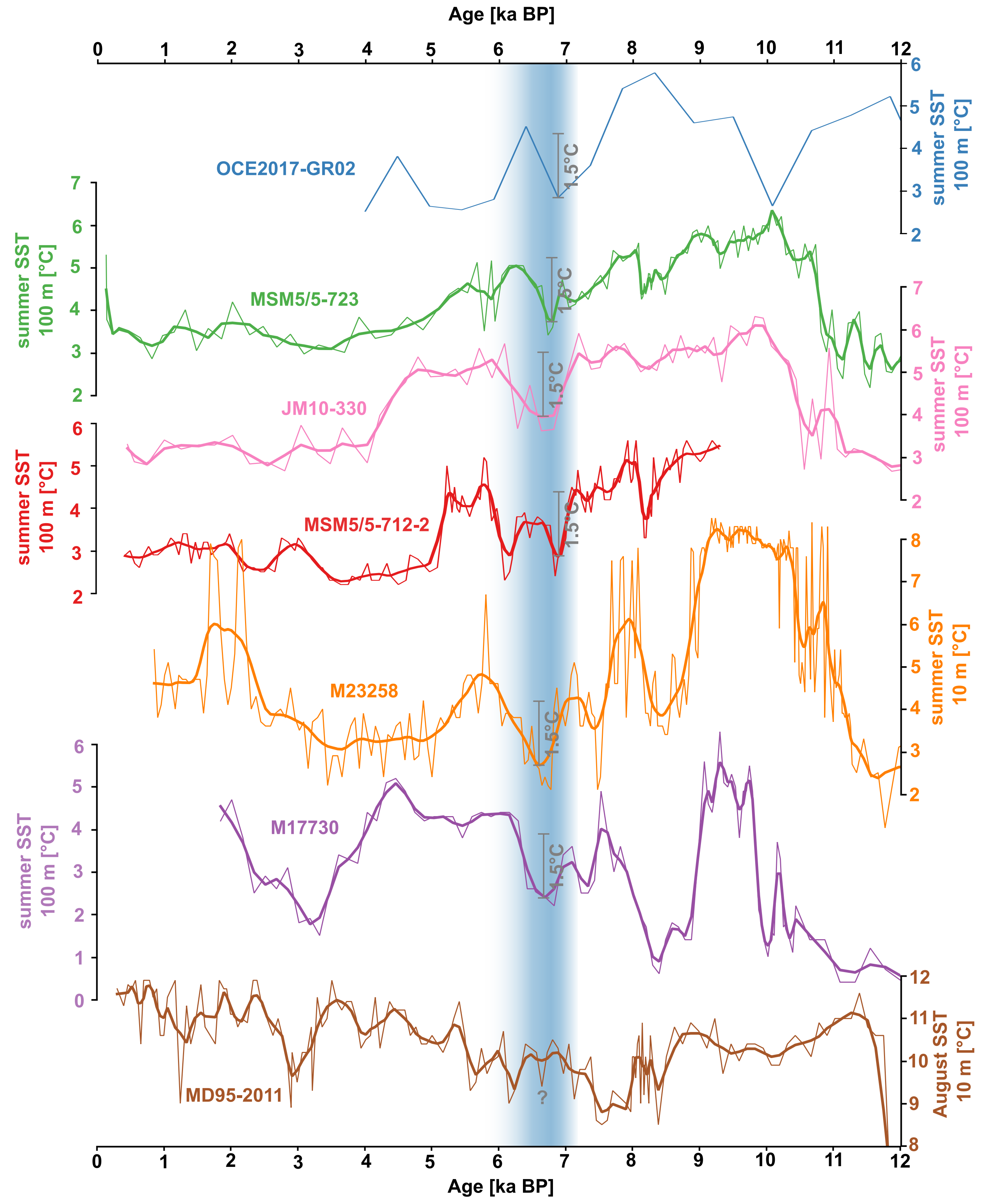

Age [ka BP]
0
1
2
3
4
5
6
7
8
9
10
11
12
OCE2017-GR02
summer SST
100 m [°C]
MSM5/5-723
JM10-330
MSM5/5-712-2
M23258
summer SST
10 m [°C]
M17730
MD95-2011
August SST
10 m [°C]
1.5°C
?

Fig. 4

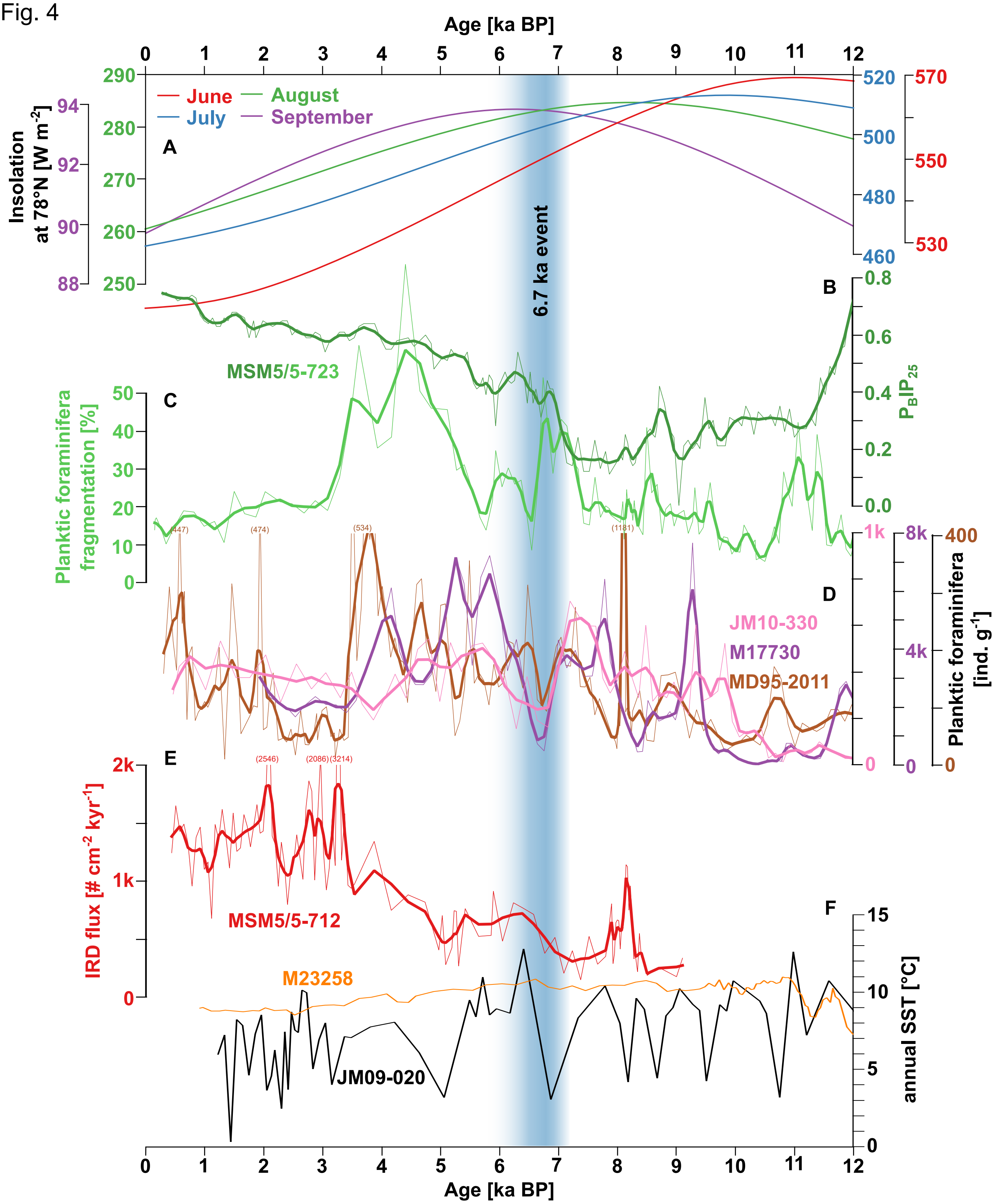

Age [ka BP]
June
July
August
September
Insolation at 78°N [W m-2]
6.7 ka event
MSM5/5-723
PBIP25
Planktic foraminifera fragmentation [%]
JM10-330
M17730
MD95-2011
Planktic foraminifera [ind. g-1]
IRD flux [# cm-2 kyr-1]
MSM5/5-712
M23258
JM09-020
annual SST [°C]
A
B
C
D
E
F

Fig. 5

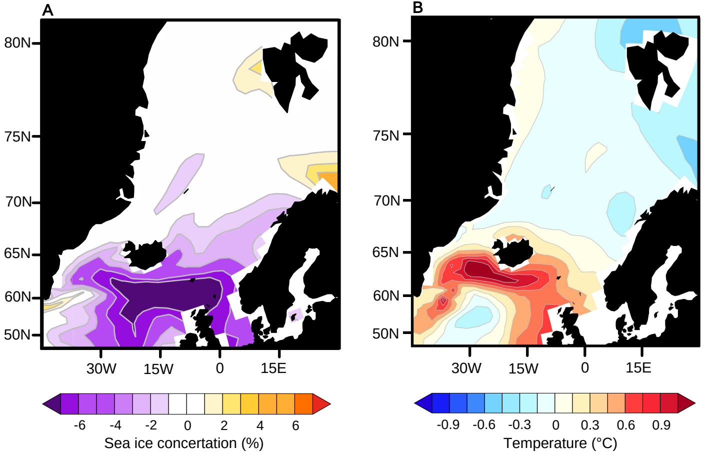
A
80N
75N
70N
65N
60N
50N
30W
15W
0
15E
-6
-4
-2
0
2
4
6
Sea ice concertation (%)
B
80N
75N
70N
65N
60N
50N
30W
15W
0
15E
-0.9
-0.6
-0.3
0
0.3
0.6
0.9
Temperature (°C)

Fig. 6

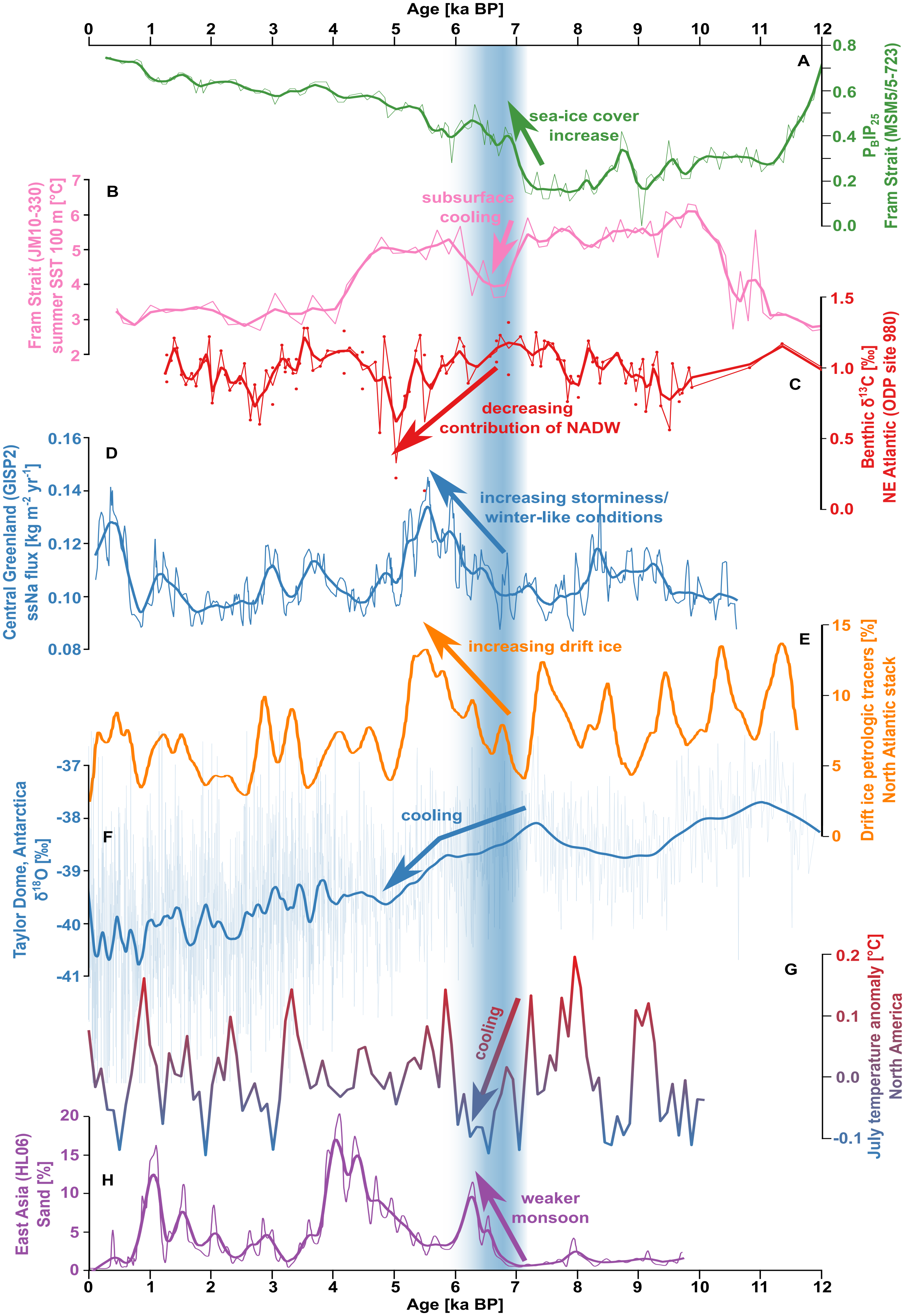

Age [ka BP]
A
B
C
D
E
F
G
H
$P_BIP_{25}$
Fram Strait (MSM5/5-723)
sea-ice cover
increase
Fram Strait (JM10-330)
summer SST 100 m [°C]
subsurface
cooling
Benthic $\delta^{13}C$ [‰]
NE Atlantic (ODP site 980)
decreasing
contribution of NADW
Central Greenland (GISP2)
ssNa flux [kg m$^{-2}$ yr$^{-1}$]
increasing storminess/
winter-like conditions
increasing drift ice
Drift ice petrologic tracers [%]
North Atlantic stack
Taylor Dome, Antarctica
$\delta^{18}O$ [‰]
cooling
July temperature anomaly [°C]
North America
cooling
East Asia (HL06)
Sand [%]
weaker
monsoon

Fig. 7

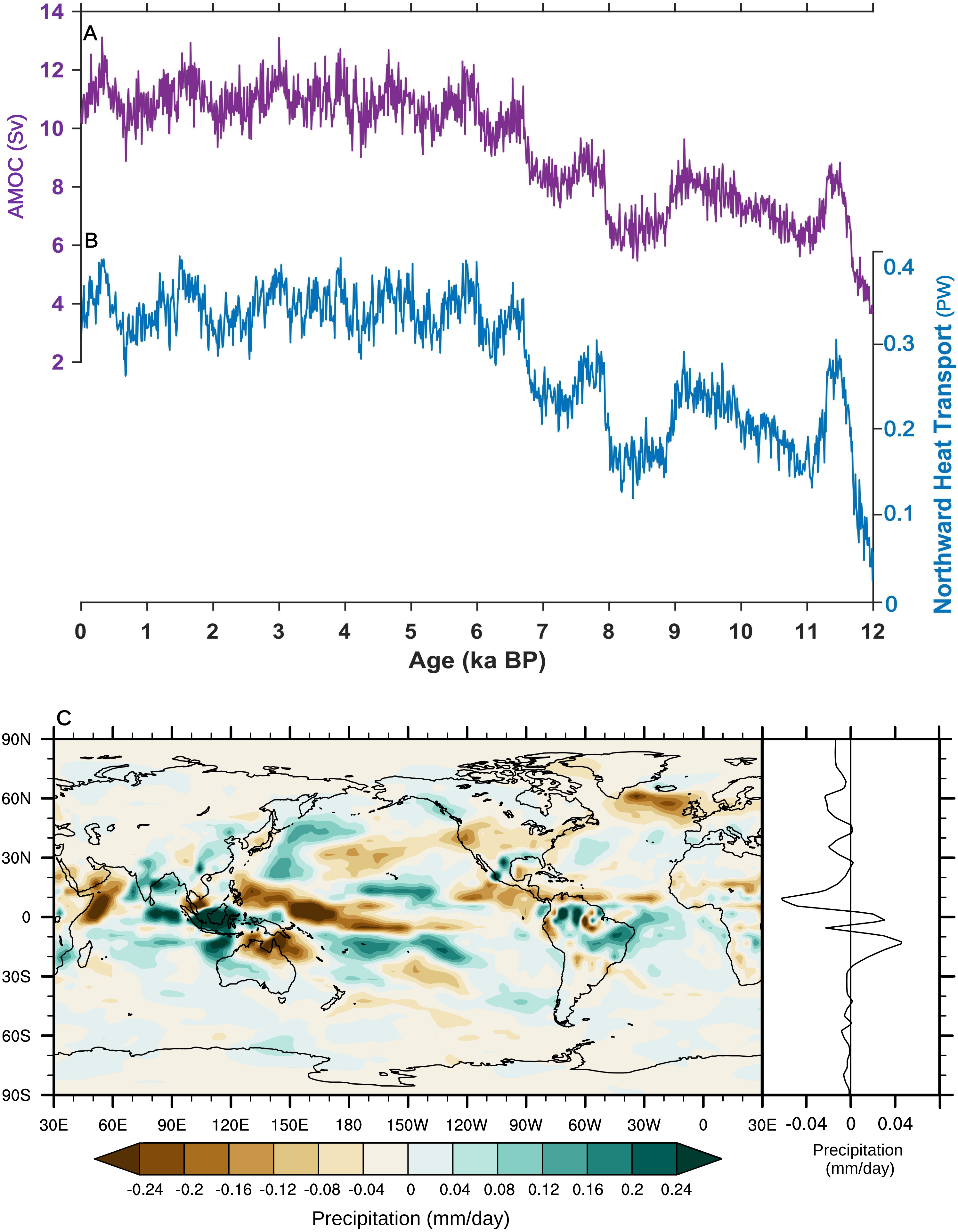
A
B
AMOC (Sv)
14
12
10
8
6
4
2
Northward Heat Transport (PW)
0.4
0.3
0.2
0.1
0
0 1 2 3 4 5 6 7 8 9 10 11 12
Age (ka BP)
C
90N
60N
30N
0
30S
60S
90S
30E 60E 90E 120E 150E 180 150W 120W 90W 60W 30W 0 30E
-0.24 -0.2 -0.16 -0.12 -0.08 -0.04 0 0.04 0.08 0.12 0.16 0.2 0.24
Precipitation (mm/day)
-0.04 0 0.04
Precipitation
(mm/day)